Electronic Supplementary Material (ESI) for Journal of Materials Chemistry A.

Supporting Information

Atomic Sn sites on nitrogen-doped carbon as zincophilic and hydrophobic protection layer for stable Zn anodes

*Yijie Wang, Yan Tan, Chuanwei Cheng**

Shanghai Key Laboratory of Special Artificial Microstructure Materials and Technology, School of Physics Science and Engineering, Tongji University, Shanghai 200092, P. R. China

* Corresponding author. Email: cwcheng@tongji.edu.cn

Experimental Section

Synthesis of nitrogen-doped carbon (NC)

3 mmol $Zn(NO)_3 \cdot 6H_2O$ was dissolved in 30 mL of methanol to form a solution A; and 12 mmol 2-Methylimidazole was dissolved in 10 mL methanol to form a solution B. Then the solution A was quickly poured in the solution B under magnetic stirring. After the solution was kept stirring for 24 h at 25 ℃, the ZIF-8 product was collected by centrifugation. The ZIF-8 powder was then annealed at 900 ℃ under Ar/H_2 atmosphere for 2 h, with a ramp rate of 5 ℃ min^{-1}. The black powder was denoted as NC.

Synthesis of atomic Sn sites anchored on nitrogen-doped carbon supports (Sn NC)

110 mg NC was dispersed in 20 mL of ethanol under ultrasonication to form a suspension C; 20 mg $SnCl_2 \cdot 2H_2O$ and 55 mg Dopamine hydrochloride were dissolved in 20 mL ethanol and 10 mL water to form a solution D. Then the solution D was added into the suspension C under magnetic stirring, and the subsequently, 750 μL $NH_3 \cdot H_2O$ was added into the mixture. The mixture was kept stirring for 12 h at 25 ℃, and the powder was collected by centrifugation, and then annealed at 900 ℃ under Ar/H_2 atmosphere for 2 h, with a ramp rate of 5 ℃ min^{-1}. The final product was denoted as Sn NC. PDA NC was synthesized for comparison by the same procedure as Sn NC without the addition of Sn precursors. The product with larger $SnCl_2$ addition (100 mg, 5 times of the amount in the synthesis of Sn NC) is denoted as Sn NC-100.

Preparation of Sn NC/Zn electrode

Commercial zinc foil with a thickness of 0.2 mm was polished with 250 and 800 grit sandpapers, respectively, to remove potential oxide layers on the surface of zinc foil. And the polished zinc foil was used as the control sample in this work. 20 mg Sn NC powder, and 20 mg Polyvinylidene fluoride (PVDF) were dispersed in 1 mL N-Methyl-2-pyrrolidone (NMP), and were stirred for 12 h for even dispersion. The mixture was coated on the polished zinc foil using a coater, and dried for 2 h at 60 ℃. The obtained composite electrode was denoted as Sn NC/Zn.

NC/Zn was prepared via a similar route, except that 20 mg PVDF was dispersed in 1 mL NMP with 20 mg NC powder.

Preparation of α-MnO_2 nanorod powder

0.5 g $MnSO_4$ were dissolved in 60 mL deionized water, and 50 μL H_2SO_4 (95-98%) was added in the solution. 20 mL 0.1 mol/L $KMnO_4$ aqueous solution was then slowly added into the solution under stirring. The mixture was then transferred into an autoclave, and kept at 120℃ for 12 h. The α-MnO_2 nanorod powder was then obtained by centrifugation, and finally dried in air under 80℃.

Characterization

Field-emission scanning electron microscope (FEI Nova Nano SEM 450) was used to observed the morphology of samples. The detailed structure information was further observed on the basis of high-resolution transmission electron microscope (Japan Electronics JEM-2100F) and high-angle annular dark-field scanning transmission electron microscope (FEI Titan Cubed Themis G2 300). The *in-situ* deposition process was observed from a customized quartz electrolyzer under an

optical microscope (Olympus BX51) and the supporting image acquisition system. The crystalline information was acquired from an X-ray diffraction (XRD) spectrometer (Bruker D8-Advance). The valence information was obtained from an X-ray photoelectron spectrometer (Thermo Fisher ESCALAB 250Xi). The information on surface area and pore sizes are based on a N_2 adsorption/desorption measurement (Micro Active for ASAP 2460, Micrometrics). Contact angles were measured via a Dataphysics OCA20 Contact Angle Measurement Instrument, and the solution was 2 M $ZnSO_4$. The contact angle was recorded immediately. The Inductively Coupled Plasma Optical Emission spectroscopy (ICP-OES) test is performed by Thermo Fisher iCAP 7400.

Electrochemical Measurements

Symmetric cells were tested in CR-2032 coin cells. Galvanostatic charge-discharge cycling was performed on a battery test system (Neware Test System, CT-3008). 2 M $ZnSO_4$ was used as electrolyte in symmetric cells, and glass fiber membranes (Whatman, 2.7 μm in pore size, 675 μm in thickness) functioned as the separators between two electrodes. Electrochemical impedance spectroscopy (EIS) with a frequency range from 0.01 Hz to 10 MHz was peformed on an electrochemical workstation (CS350, Wuhan Corrtest) and the fitting process was based on Zview software. Linear sweep voltammetry (LSV) were measured on an electrochemical workstation (CHI760D, Shanghai, Chenhua Co., China). The LSV measurement was based on a potential range of -0.7 ~ -1.6 V in a three-electrode system in 2 M $ZnSO_4$,

wherein Ag/AgCl electrode was used as the reference electrode, and samples with an area of 0.5 cm^{-2} were used for both working electrode and counter electrode.

Zn//MnO_2 full batteries were tested in CR-2032 coin cells, wherein the as-prepared composite electrodes, Sn NC/Zn, NC/Zn and Zn foil, were used as anodes, and 2 M $ZnSO_4$-0.2 M $MnSO_4$ functioned as the electrolyte. Cyclic voltammetry profiles were obtained on an electrochemical workstation (CHI760D, Shanghai, Chenhua Co., China), with a potential range of 0.8-1.8 V at a sweeping rate of 0.2 mV s^{-1}. Long-term cycling was tested on a battery test system (Neware Test System, CT-3008). The α-MnO_2 cathode was prepared by mixing α-MnO_2 powder (70 wt%), acetylene black (20 wt%), and polyvinylidene fluoride (10 wt%). The mixture was coated on a pretreated titanium foil and dried at 80℃ for 12 h. The average mass loading on a titanium foil was 1.9 mg cm^{-2}.

Zn//MnO_2 pouch cells were sealed by aluminum plastic film with a vacuum heat sealer. MnO_2 cathode and Sn NC/Zn anode were cut into a size of 3*3 cm^{-2}, and were attached with a nickel tab by conductive silver paste, respectively. The separator was glass fiber membranes (Whatman, 2.7 μm in pore size, 675 μm in thickness) with a size of 3.5*3.5 cm^{-2}. The mass loading of MnO_2 for pouch cells is the same as that for coin cells, which is ~1.9 mg cm^{-2}. The electrolyte amount for pouch cells is 2 mL of 2 M $ZnSO_4$ and 0.2 M $MnSO_4$.

Simulation of electric field distribution and concentration distribution

A two-dimensional electrochemistry module was called in COMSOL Multiphysics 5.6 to simulate the electric field and the concentration distribution at the solid/liquid

interface near the anodes. The size of the model was 9×7 μm^2. The size of Sn NC and NC particles are determined based on TEM results, with a diameter of 750 nm. The ionic conductivity of 2 M $ZnSO_4$ electrolyte was determined to be 5 S m^{-1}. The values for electrical conductivity of zinc metal, nitrogen-doped carbon, and Sn metal were set to be 1.67×10^7, 3×10^5, and 9.17×10^6 S m^{-1}, respectively. An overpotential of 500 mV was applied as the excitation between top and bottom boundaries. The simulated current density was normalized, and the remaining boundary was set to be in insulation. The *j*, *J, and c* here are the calculated current density, Zn ion flux, the electrolyte concentration, respectively. The j_0, J_0, *and* c_0 here are the highest calculated current density, Zn ion flux, the electrolyte concentration, respectively. The diffusion coefficient of Sn-N-C layer, NC are determined as 3×10^{-10} m^2 s^{-1}, and 1×10^{-9} m^2 s^{-1}, respectively, which is generally in correspondence with the hydrophobicity of materials. The initial concentration of $ZnSO_4$ electrolyte is 2000 mol m^{-3}.

Theoretical calculation

To calculate the adsorption energy, *Density Functional Theory* (DFT) calculations are employed, which is based on the *projector augmented-wave* method in *Vienna ab initio simulation package* (VASP).The *Generalized Gradient Approximation* (GGA) with *Perdew-Burke-Ernzerhof* (PBE) pseudopotential was adopted to describe the exchange-correlation interactions of electron. The *Gamma* scheme with a 2*2*1 *k*-point mesh was applied, for integration in the irreducible *Brillouin zone*. Cut-off energies of 400 eV (for structural optimization calculation) and 450 eV (for total

energy calculation) were used for the plane wave expansion. The total energy was converged below $1*10^{-4}$ eV with a final force convergence fewer than 0.01 eV/Å. The supercell of graphene and bulk models including cells with 6*6 unit was built and vacuum layer of 35 Å was carried out to avoid interaction between two adjacent unit cells. The adsorption energy (E_{ads}) of Zn is defined as

$$E_{ads} = E_{surf+Zn} - E_{Zn} - E_{surf} \quad (1)$$

Wherein E_{surf} is the surface energy. E_{Zn} represents the energy of a Zn atom and $E_{surf+Zn}$ stands for the total energy of Zn adsorbed onto the corresponding surface. The real-space interfacial charge density distribution was visualized in VESTA.

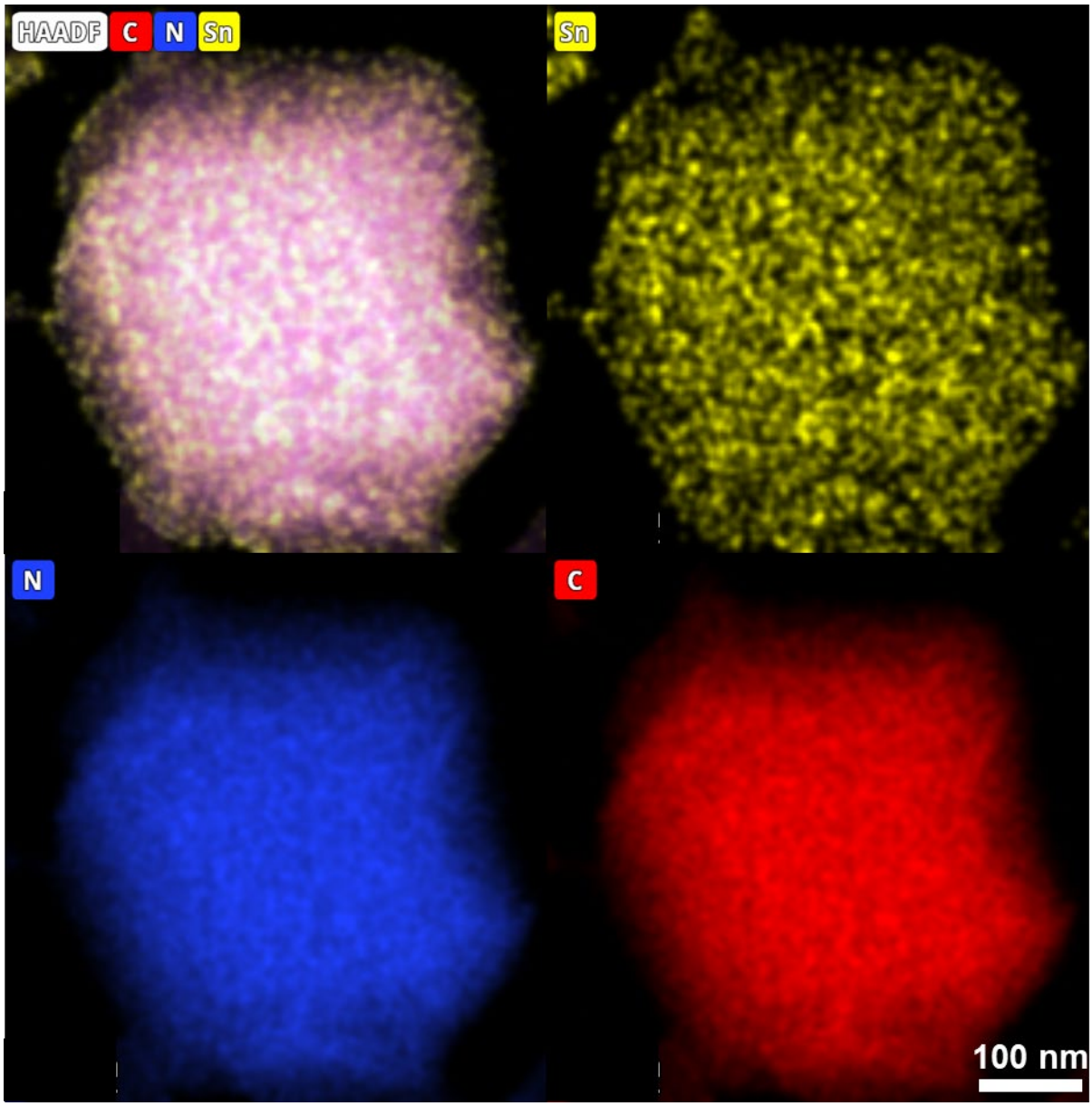

Figure S1 Element mappings of (a) overlapped element distribution, (b) Sn, (c) N, and (d) C.

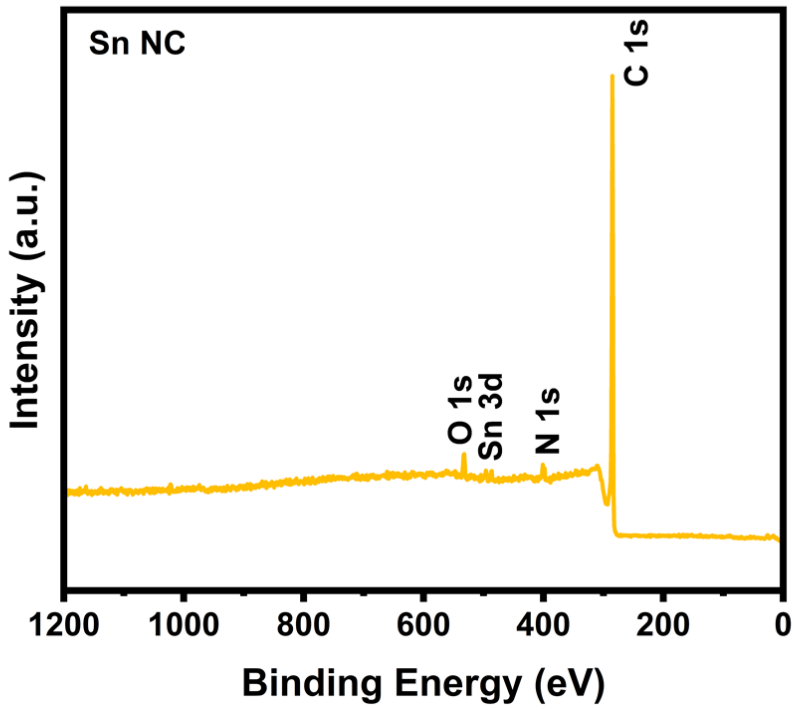

Figure S2 XPS overall spectrum of Sn NC

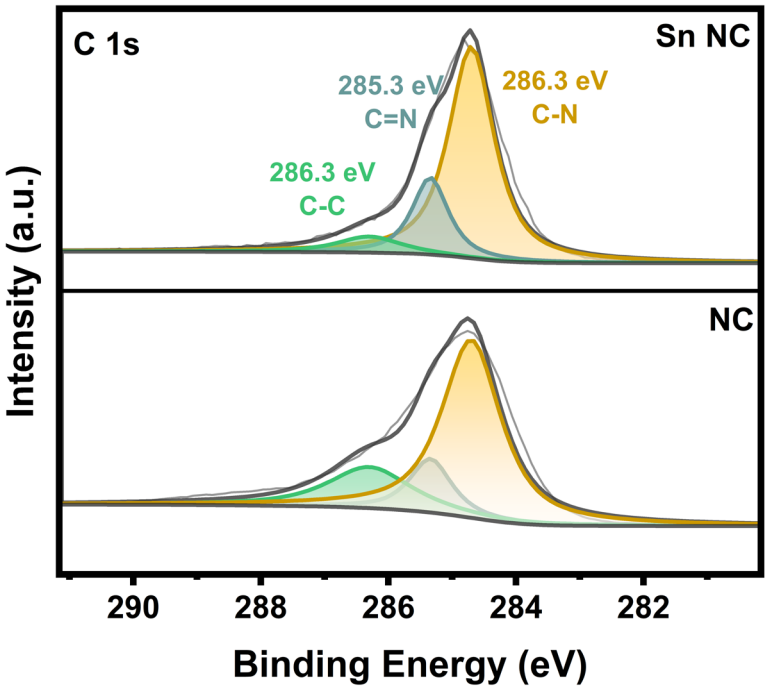

Figure S3 C 1s spectra of Sn NC and NC

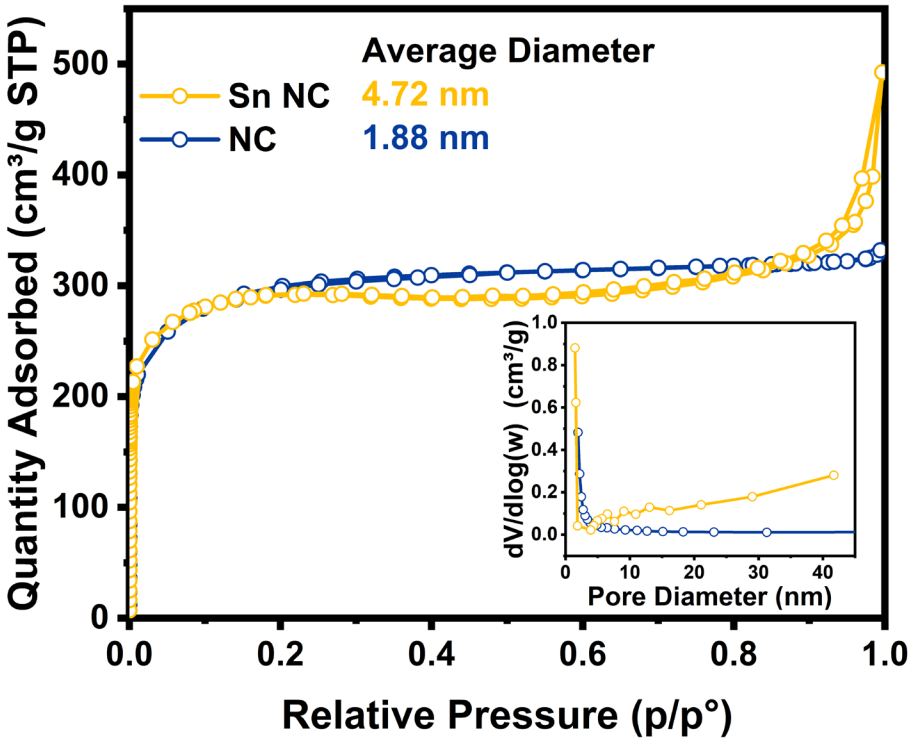

Figure S4 BET surface area profiles of Sn NC and NC (pore size distribution profiles in inset)

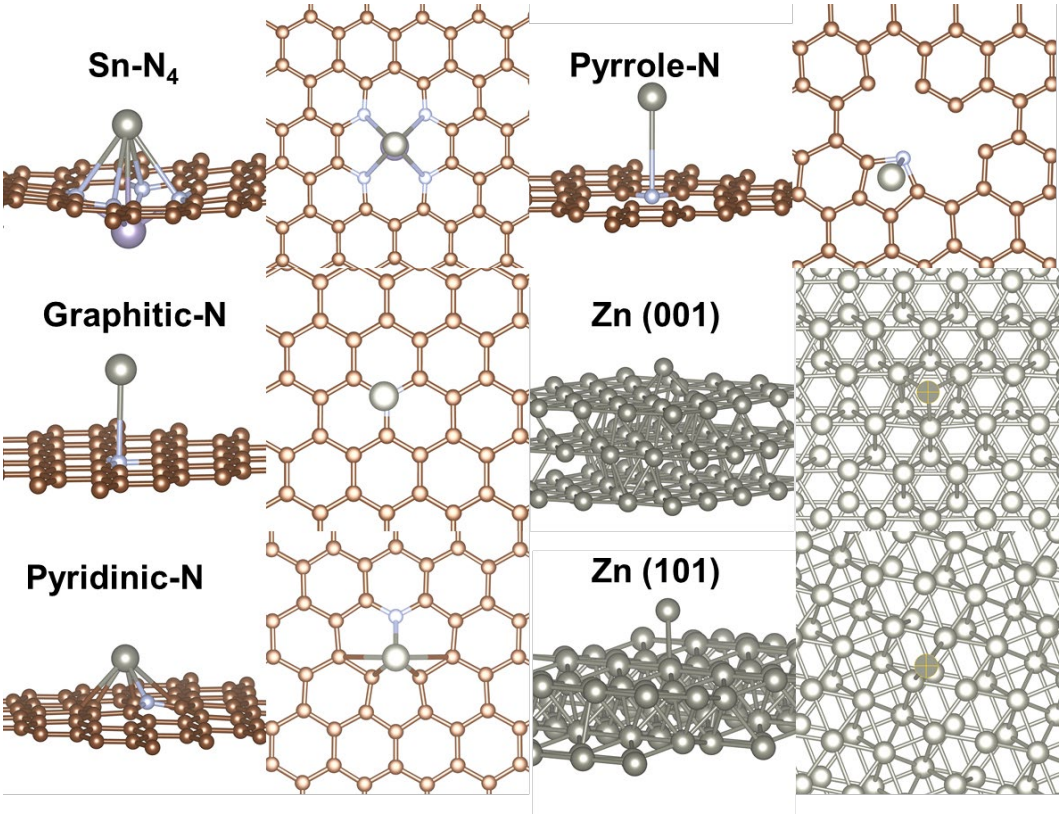

Figure S5 Modeling of Zn atom with different configurations in DFT calculations.

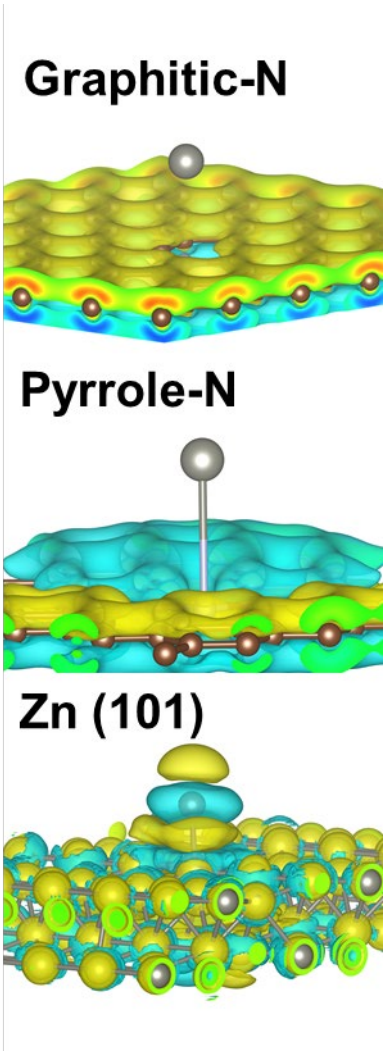

Figure S6 Interfacial charge-density models of Zn atom with Graphitic-N, Pyrrole-N, and Zn (101).

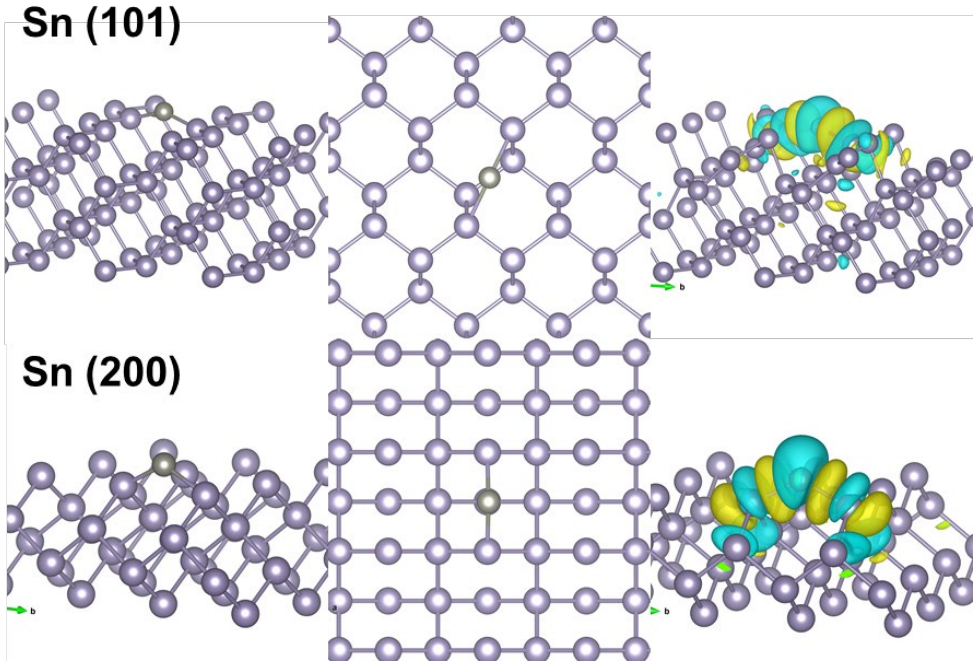

Figure S7 Models and interfacial charge-density models of Zn atom with Sn (101) and Sn (200).

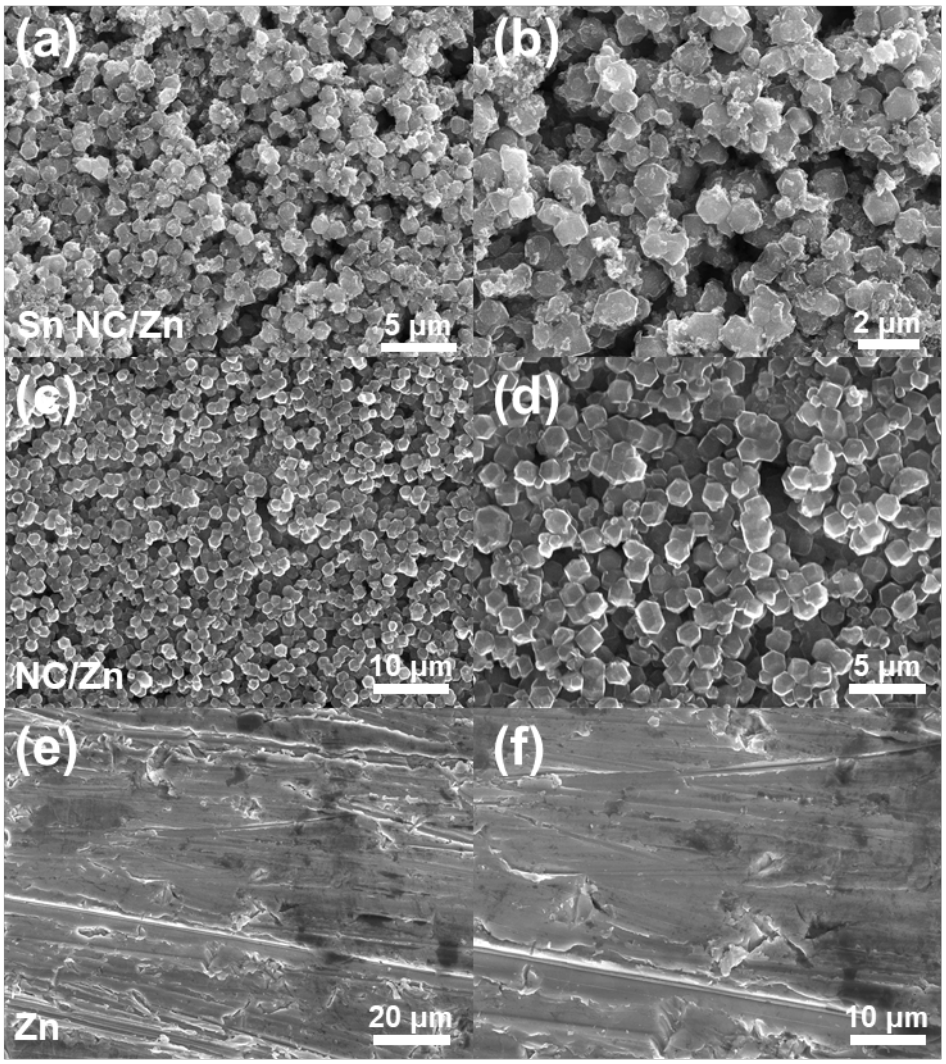

Figure S8 SEM images of (a, b) Sn NC/Zn, (c, d) NC/Zn, and (e, f) Zn

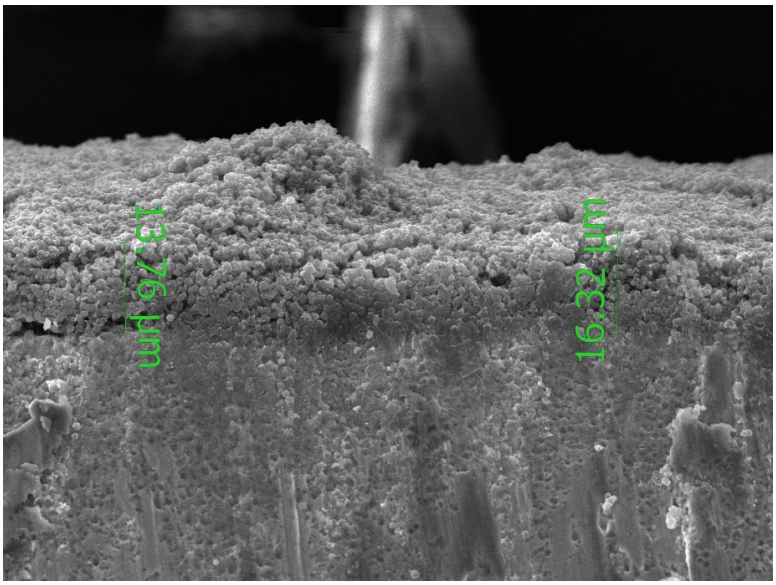

Figure S9 SEM cross-sectional image of Sn NC/Zn.

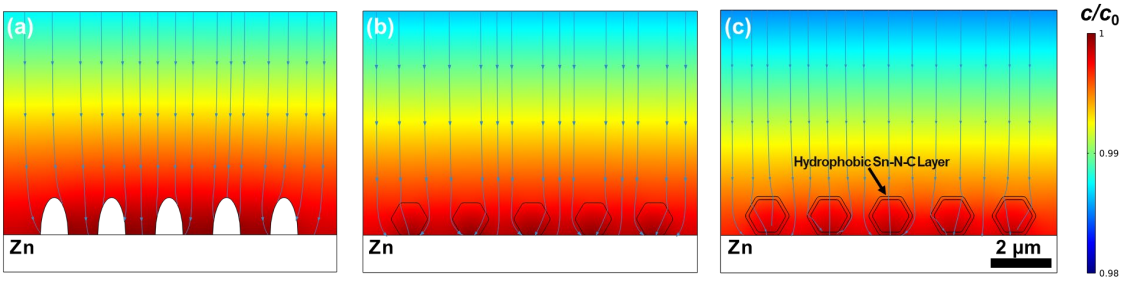

Figure S10 Concentration distribution simulation of Zn, NC/Zn, and Sn NC/Zn.

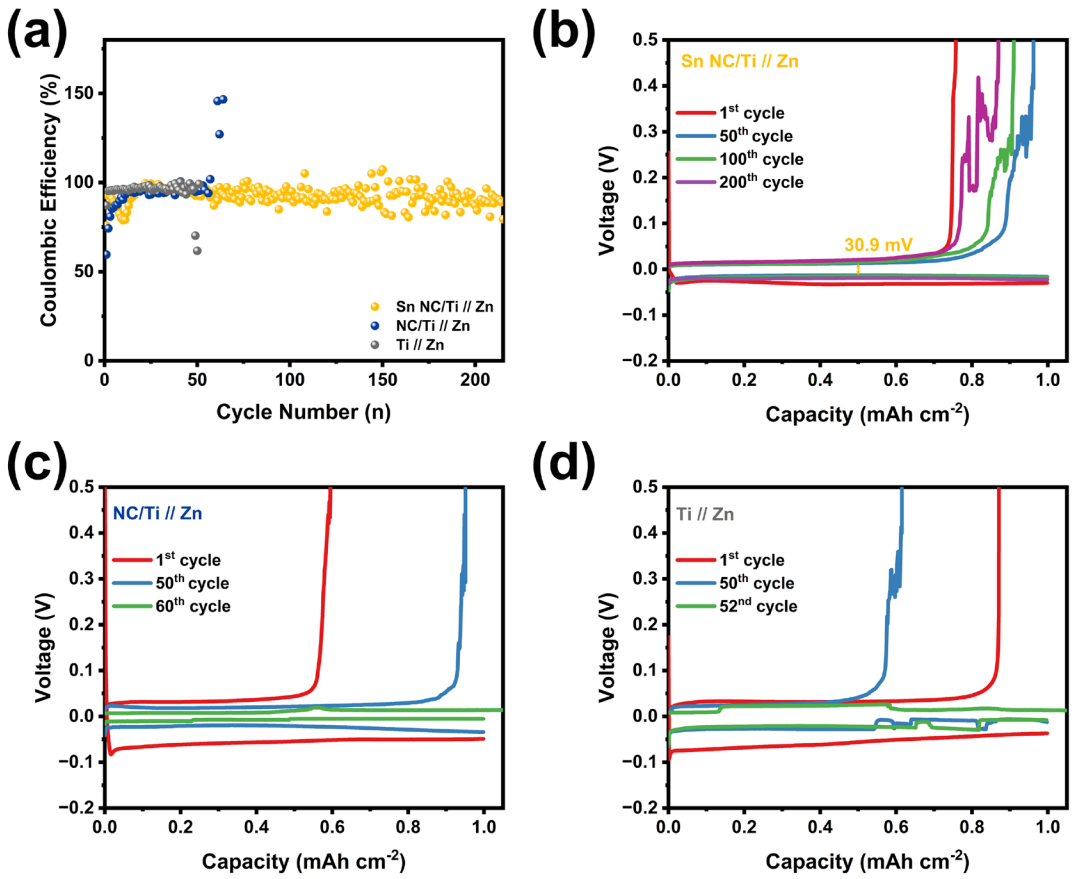

Figure S11 Coulombic efficiency (a) and charge/discharge profiles at selected cycles of (b) Sn NC/Ti, (c) NC/Ti and (d) Ti in Ti//Zn asymmetric cells

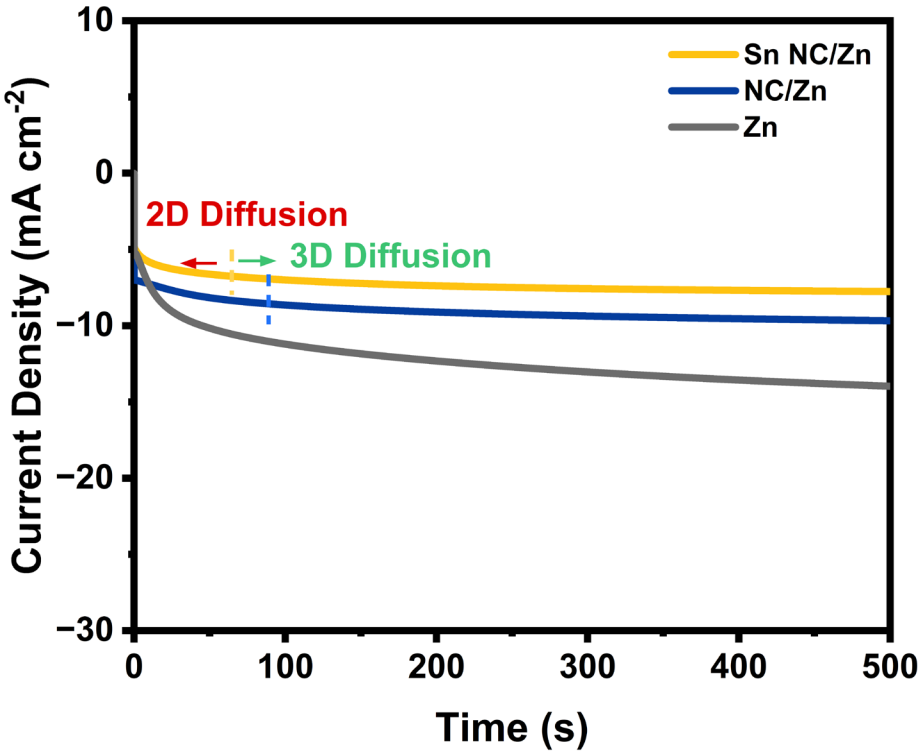

Figure S12 Chronoamperometry curves of Sn NC/Zn, NC/Zn, and Zn.

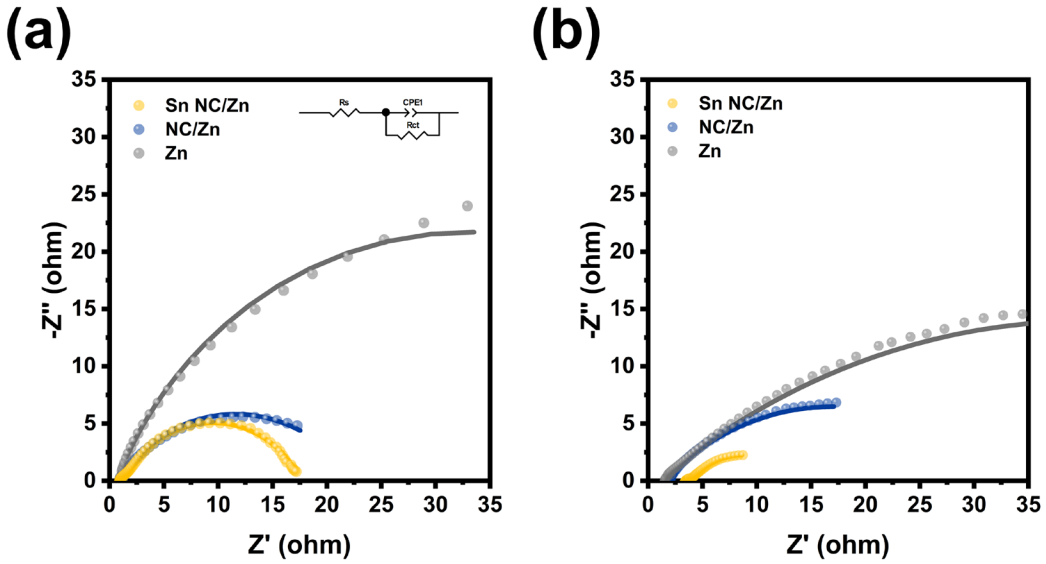

Figure S13 Nyquist plots at high frequency region of Sn NC/Zn, NC/Zn, and Zn in symmetric cells (a) before cycling and (b) after 50 cycles at 1 mA cm^{-2} and 1 mAh cm^{-2}. Dots are the original data while lines represent the fitted curves.

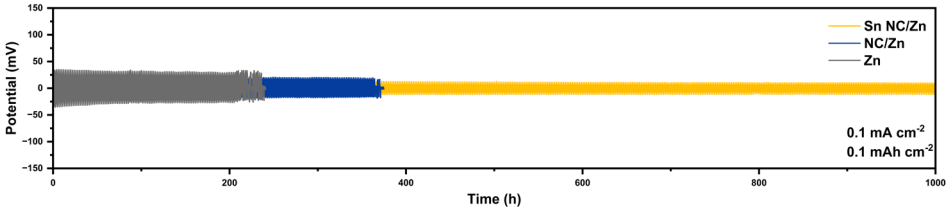

Figure S14 Cycling profiles of Sn NC/Zn, NC/Zn, and Zn in symmetric cells at 0.1 mA cm^{-2}, 0.1 mAh cm^{-2}

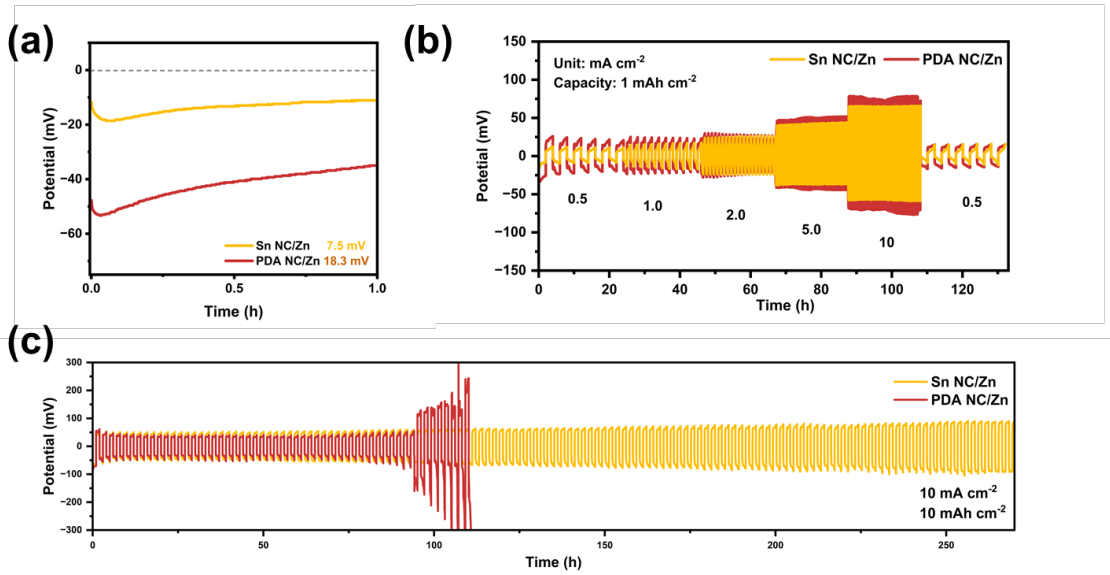

Figure S15 (a) Nucleation overpotential profiles in symmetric cells at 1 mA cm^{-2} and 1 mAh cm^{-2}; (b) rate performance; and (c) long-term cycling at 10 mA cm^{-2} and 10 mAh cm^{-2} of Sn NC/Zn, PDA NC/Zn.

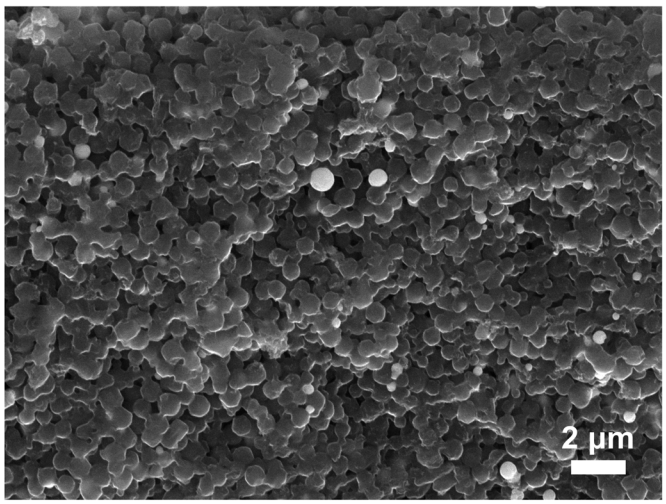

Figure S16 SEM images of Sn NC-100.

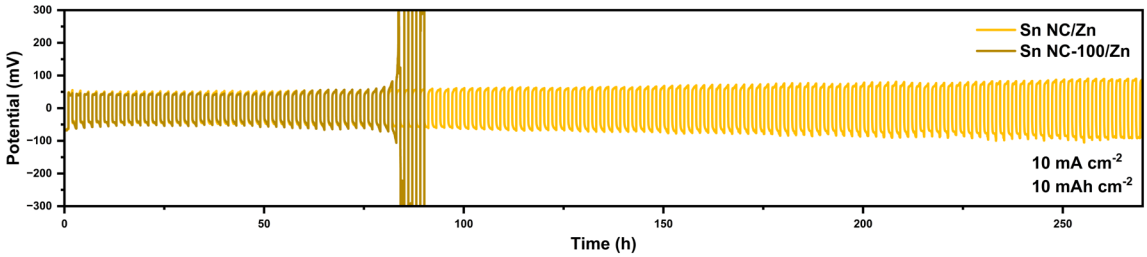

Figure S17 Long-term cycling at 10 mA cm^{-2} and 10 mAh cm^{-2} of Sn NC/Zn, Sn NC-100/Zn.

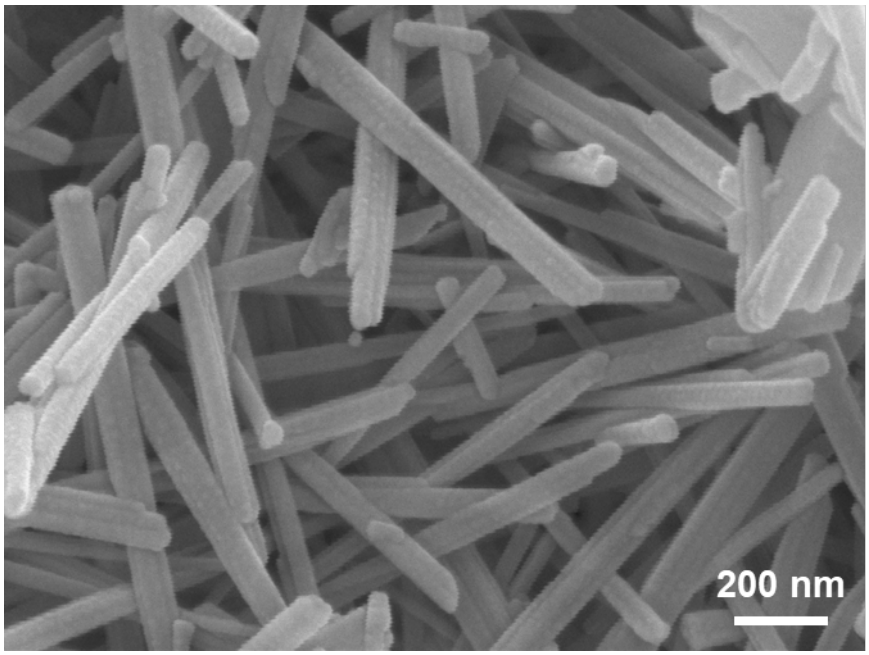

Figure S18 SEM image of MnO_2 nanorods

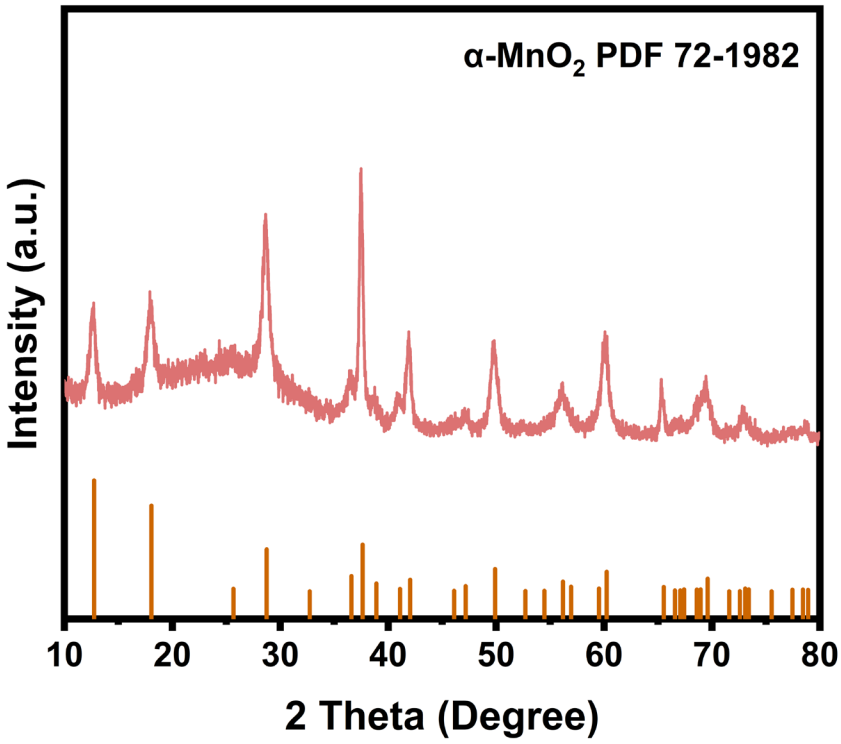

Figure S19 XRD spectrum of MnO_2 nanorods

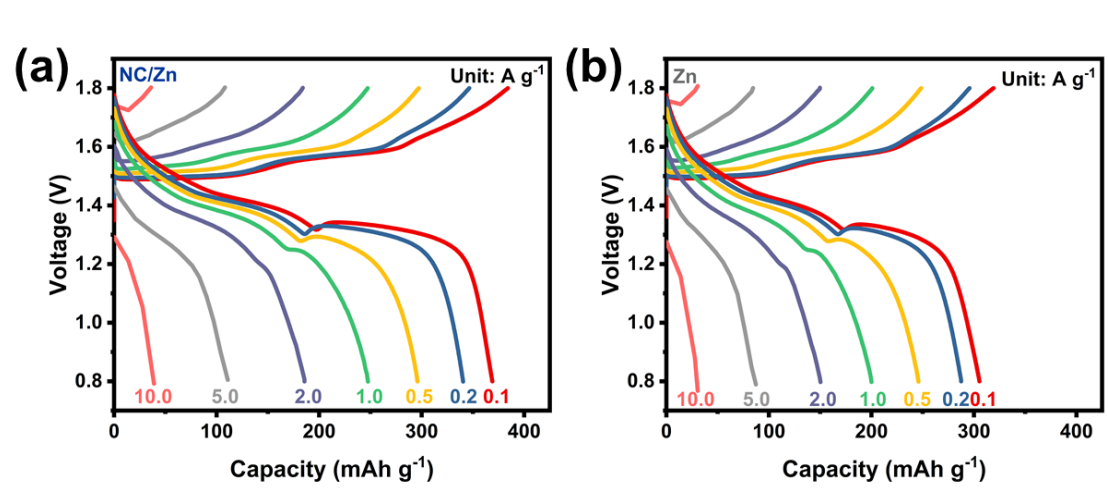

Figure S20 Charge/discharge profiles at different rates of (a) NC/Zn and (b) Zn in MnO_2//Zn full batteries

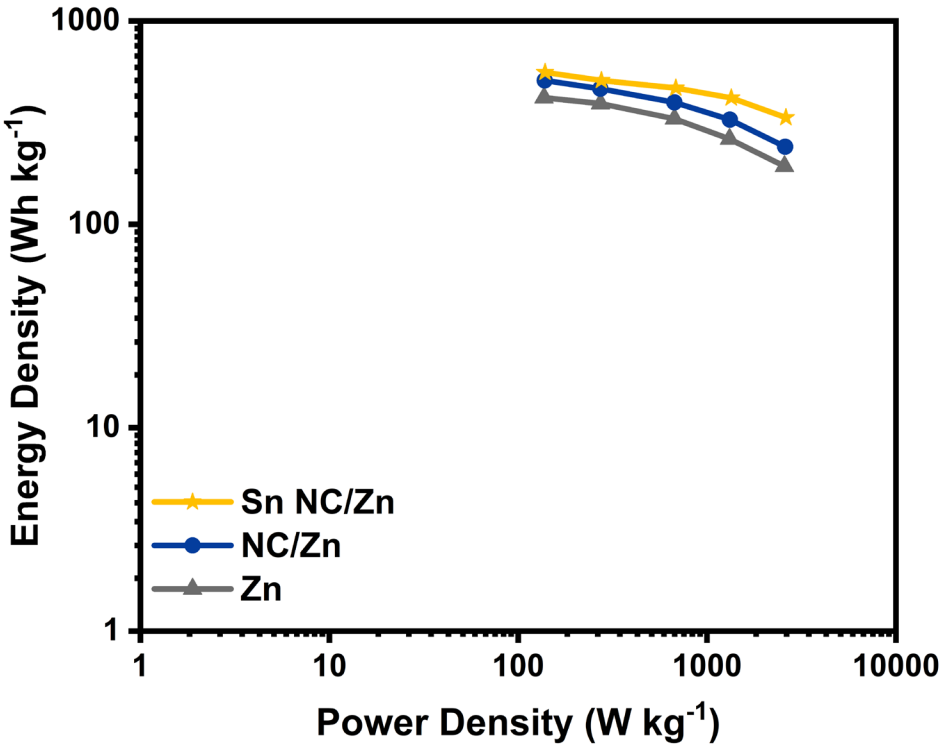

Figure S21 Ragone plots of Sn NC/Zn, NC/Zn, and Zn in MnO_2//Zn full batteries.

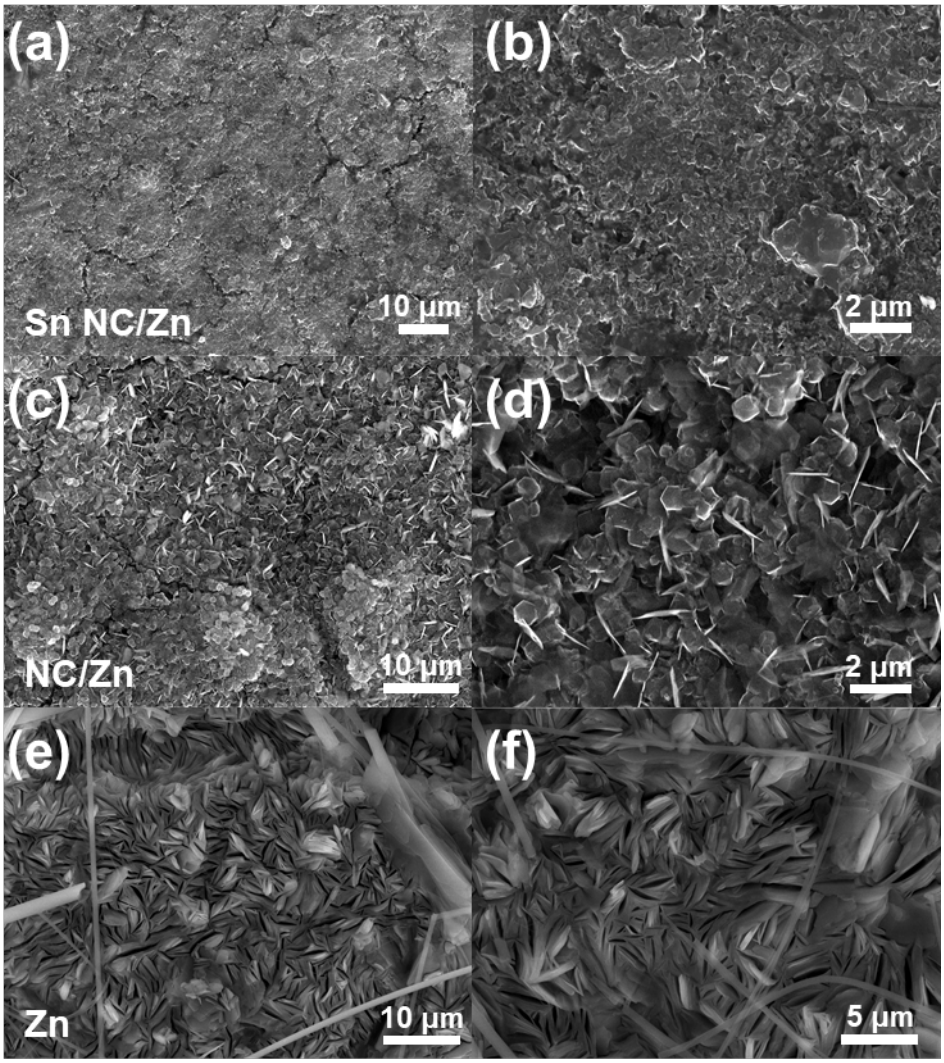

Figure S22 SEM images of (a, b) Sn NC/Zn, (c, d) NC/Zn, and (e, f) Zn after cycling in MnO_2//Zn full batteries

Table S1 Comparison of cycling performance of symmetric cells in recently-reported literatures

Sample	Electrolyte	Current density (mA cm^{-2})	Areal capacity (mAh cm^{-2})	Overpotential (mV)	Voltage hysteresis (mV)	Cycling Time (h)	Reference
Sn NC/Zn	2 M $ZnSO_4$	0.1	0.1	11.4	22.2	1000	This Work
		1	1	23.8	49.8	1000	
		10	10	77.8	145.9	280	
NCL-Zn	2 M $ZnSO_4$	1	1	/	90	4000	[1]
Zn|Sn	2 M $ZnSO_4$	1	0.5	/	46.3	2200	[2]
MIL-125(Ti)-Zn	3 M $ZnSO_4$	1	1	/	80	2100	[3]
Cu NBs@NCFs -Zn	2 M $ZnSO_4$	2	1	/	34.6	450	[4]
ZnSnN	2 M $ZnSO_4$	0.5	0.5	/	~40	1200	[5]
		5	1	/	~137	500	
Sn-	2 M	1	1	22	/	750	[6]

PCF@Zn	$ZnSO_4$	10	5	47	/	500	
Zn@PDA	2 M $ZnSO_4$	0.5	0.25	/	42	200	7
CF-Cu@Zn	2 M $ZnSO_4$	0.5	0.25	14.6	/	2200	8
ZnSn-1	2 M $ZnSO_4$	5	5	75	/	240	9
Bi-N_4/C	2 M $ZnSO_4$	0.5	1	/	82	350*	10
	$Zn(OTF)_2$	5	1	/	142	600	
Zn@ZnSe	2 M $ZnSO_4$	1	1	28	/	1500	11
		10	1	82	/	1500	

* including a rate test with a fixed capacity of 1 mAh cm^{-2}.

Table S2 Comparison of cycling performance of full batteries in recently-reported literatures

Anode	Cathode	Rate (A g^{-1})	Cycles	Final Capacity (mAh g^{-1})	Capacity Retention (%)	Reference
Sn NC/Zn	α-MnO_2	2	2800	76.2	50.6	This work
Cu NBs@NCFs-Zn	Mn_2O_3-$ZnMn_2O_4$	1	2000	130.4	67.6	[4]
Sn-PCF@Zn	NaVO	5	2000	150	~57%	[6]
Zn@PDA	MnO_2	1	1000	~100	~74	[7]
CF-Cu@Zn	V_2O_5	3	2500	~104	~53	[8]
Zn@ZnSe	MnO_2	0.616	1800	~71.4	~36	[11]
Sn-Zn	NaV_3O_8*1.5H_2O	1	600	~80	70	[12]

References

1. Y. Li, D. Zhao, J. Cheng, Y. Lei, Z. Zhang, W. Zhang and Q. Zhu, A bifunctional nitrogen doped carbon network as the interlayer for dendrite-free Zn anode, *Chem. Eng. J.*, 2023, **452**, 139264, 10.1016/j.cej.2022.139264.
2. M. Zhou, C. Fu, L. Qin, Q. Ran, S. Guo, G. Fang, X. Lang, Q. Jiang and S. Liang, Intrinsic structural optimization of zinc anode with uniform second phase for stable zinc metal batteries, *Energy Storage Mater.*, 2022, **52**, 161-168, 10.1016/j.ensm.2022.06.058.
3. C. Zhao, Y. Du, Z. Guo, A. Chen, N. Liu, X. Lu, L. Fan, Y. Zhang and N. Zhang, Missing-linker bifunctional MIL-125(Ti)-Zn interface modulation layer to simultaneously suppress hydrogen evolution reaction and dendrites for Zn metal anodes, *Energy Storage Mater.*, 2022, **53**, 322-330, 10.1016/j.ensm.2022.09.014.
4. Y. Zeng, P. X. Sun, Z. Pei, Q. Jin, X. Zhang, L. Yu and X. W. D. Lou, Nitrogen-Doped Carbon Fibers Embedded with Zincophilic Cu Nanoboxes for Stable Zn-Metal Anodes, *Adv. Mater.*, 2022, **34**, 2200342, 10.1002/adma.202200342.
5. S. Zhai, X. Shi, K. Jiang, X. Tan, W. Zhang, J. Zhang, H. Zhang and Z. Li, Flame normalizing-induced robust and oriented metallic layer for stable Zn anode, *Chem. Eng. J.*, 2022, **437**, 135246, 10.1016/j.cej.2022.135246.
6. J.-L. Yang, P. Yang, W. Yan, J.-W. Zhao and H. J. Fan, 3D zincophilic micro-scaffold enables stable Zn deposition, *Energy Storage Mater.*, 2022, **51**, 259-265, 10.1016/j.ensm.2022.06.050.
7. T. Wang, P. Wang, L. Pan, Z. He, L. Dai, L. Wang, S. Liu, S. C. Jun, B. Lu, S. Liang and J. Zhou, Stabling Zinc Metal Anode with Polydopamine Regulation through Dual Effects of Fast Desolvation and Ion Confinement, *Adv. Energy Mater.*, 2022, **13**, 2203523, 10.1002/aenm.202203523.
8. H. Wang, Y. Chen, H. Yu, W. Liu, G. Kuang, L. Mei, Z. Wu, W. Wei, X. Ji, B. Qu and L. Chen, A Multifunctional Artificial Interphase with Fluorine-Doped Amorphous Carbon layer for Ultra-Stable Zn Anode, *Adv. Funct. Mater.*, 2022, **32**, 2205600, 10.1002/adfm.202205600.
9. L. Wang, W. Huang, W. Guo, Z. H. Guo, C. Chang, L. Gao and X. Pu, Sn Alloying to Inhibit Hydrogen Evolution of Zn Metal Anode in Rechargeable Aqueous Batteries, *Adv. Funct. Mater.*, 2021, **32**, 2108533, 10.1002/adfm.202108533.
10. S. Chen, J. Chen, X. Liao, Y. Li, W. Wang, R. Huang, T. Zhao, S. Yan, Z. Yan, F. Cheng and H. Wang, Enabling Low-Temperature and High-Rate Zn Metal Batteries by Activating Zn Nucleation with Single-Atomic Sites, *ACS Energy Lett.*, 2022, **7**, 4028-4035, 10.1021/acsenergylett.2c02042.
11. L. Zhang, B. Zhang, T. Zhang, T. Li, T. Shi, W. Li, T. Shen, X. Huang, J. Xu, X. Zhang, Z. Wang and Y. Hou, Eliminating Dendrites and Side Reactions via a Multifunctional ZnSe Protective Layer toward Advanced Aqueous Zn Metal Batteries, *Adv. Funct. Mater.*, 2021, **31**, 2100186, 10.1002/adfm.202100186.
12. Z. Miao, M. Du, H. Li, F. Zhang, H. Jiang, Y. Sang, Q. Li, H. Liu and S. Wang, Constructing nano-channeled tin layer on metal zinc for high-performance zinc-ion batteries anode, *EcoMat*, 2021, **3**, 12125, 10.1002/eom2.12125.